NUCL SCI TECH (2019) 30:48
https://doi.org/10.1007/s41365-019-0575-5

Neutronic analysis of silicon carbide cladding accident-tolerant fuel assemblies in pressurized water reactors

Zhi-Xiong Tan[1] · **Jie-Jin Cai**[1]

Received: 3 March 2018 / Revised: 25 July 2018 / Accepted: 13 September 2018 / Published online: 14 February 2019

Abstract In resonance with the Fukushima Daiichi Nuclear Power Plant accident lesson, a novel fuel design to enhance safety regarding severe accident scenarios has become increasingly appreciated in the nuclear power industry. This research focuses on analysis of the neutronic properties of a silicon carbide (SiC) cladding fuel assembly, which provides a greater safety margin as a type of accident-tolerant fuel for pressurized water reactors. The general physical performance of SiC cladding is explored to ascertain its neutronic performance. The neutron spectrum, accumulation of ^{239}Pu, physical characteristics, temperature reactivity coefficient, and power distribution are analyzed. Furthermore, the influences of a burnable poison rod and enrichment are explored. SiC cladding assemblies show a softer neutron spectrum and flatter power distribution than conventional Zr alloy cladding fuel assemblies. Lower enrichment fuel is required when SiC cladding is adopted. However, the positive reactivity coefficient associated with the SiC material remains to be offset. The results reveal that SiC cladding assemblies show broad agreement with the neutronic performance of conventional Zr alloy cladding fuel. In the meantime, its unique physical characteristics can lead to improved safety and economy.

This work was supported by the National Natural Science Foundation of China (No. 11675057) and the Fundamental Research Funds for the Central Universities (No. 2017ZD100).

✉ Jie-Jin Cai
epjjcai@scut.edu.cn

[1] School of Electric Power, South China University of Technology, Guangdong 510640, China

Keywords Accident-tolerant fuels · Silicon carbide cladding · Neutronic characteristics · Pressurized water reactor

1 Introduction

When beyond design basis accident (BDBA) scenarios occur, such as the Fukushima Daiichi Nuclear Power Plant accident, with loss of active cooling, conventional Zr alloy cladding fuel in pressurized water reactors (PWRs) is expected to provide a safety margin. Many institutions have made efforts to design accident-tolerant fuel (ATF) to satisfy these high safety demands [1, 2]. Many concepts, which have primarily focused on improving fuel pellet characteristics, applying external coating, and replacing the conventional cladding with alternative materials, have been evaluated with respect to ATF.

Neutronic evaluation is crucial for assessing the safety and economy of ATF. Represented by Oak Ridge National Laboratory, analysis of fully ceramic microencapsulated (FCM) fuel at the lattice level and nodal full reactor simulation was carried out from the aspect of cycle length, temperature coefficient, and transient response [3, 4]. The neutronic feasibility of using a novel uranium mononitride (UN) fuel in a light water reactor (LWR) has been verified [5]. Substitutive cladding and external coating material under normal operation conditions have also been evaluated. FeCrAl cladding design shows preferable characteristics, including a flattened axial temperature profile and delayed gap closure [6]. Austenitic type 310 (310SS), 304 stainless steels, silicon carbide (SiC), and advanced molybdenum alloy (TZM) have involved in neutronic parametric assessment as cladding material [7, 8]. Thermal

and cold spray techniques have been adopted to coat a MAX phase (like Ti_3AlC_2) on zirconium alloy cladding [9] and a TiAlN coating on ZIRLO fuel cladding [10]. Simulation of transient accidents has been carried out to investigate the behavior of an ATF-loaded reactor [11, 12].

SiC cladding is included in the list of ATF concepts because of its extraordinary oxidation resistance capacity, chemical inertia, and other relevant strengths [13, 14]. Related research has been carried out at the Massachusetts Institute of Technology [15, 16]. Critical nuclear reactivity experiments for SiC material have been implemented as a foundation for numerical simulation [17]. We also completed neutronic analyses of ATF assemblies with SiC cladding in pressurized water reactors and pressurized water reactor core loading with SiC cladding fuels. In this paper, we will provide a detailed summary of the results of our research on the characteristics of SiC cladding ATF assemblies in PWRs from the viewpoint of neutronics.

The remaining paper is organized as follows. Section 2 gives a description of the material compositions of the ATF assembly and some primary parameters for the neutron physical model. The results of the neutronic performance of the assemblies are addressed in Sect. 3. The conclusion is provided in Sect. 4.

2 Models and technical parameters

The open-source lattice calculation code "DRAGON" was employed for neutronic physics calculation. As a fully functional lattice cell code, it includes various integral transport equation solutions [18]. It is a full-scale lattice cell code made at the Institute of Nuclear Engineering of Polytechnique Montréal, Canada, with different algorithms to solve transport-diffusion equivalence, homogenizing group constants, and isotopic depletion calculations. We have used the code to successfully analyze the neutronic characteristics of SCWRs and PWRs [19–21]. Also, the DRAGON code has been used to analyze the neutronic properties of the CANDU-6 reactor [22]. In this paper, a collision probability algorithm was chosen for solving the neutron transport equation, and the generalized Stamm'ler method was used to consider the resonance self-shielding.

2.1 Rationale for using SiC

SiC has potential material characteristic advantages over zirconium alloy, among which are sufficient resistance to oxidation and creep, irradiation stability, attractive thermal endurance, and low thermal neutron capture cross sections. SiC has excellent compatibility with UO_2, moderators, and coolant under operation conditions. Even in accident scenarios, it would avoid hydrogen explosion. On the occasion of volumetric swelling saturation caused by irradiation, SiC remains highly resistant to a high fast flux [23]. Neutronic irradiation has a minimum effect on SiC, except for the thermal conductivity. Compared with Zr alloy, SiC has been shown to have a superior antioxidant ability [24, 25].

2.2 Physical design of assemblies

Figure 1 shows the typical 17 × 17 assembly layout without a burnable poison rod. The blue dots represent fuel cells, while the white ones correspond to guide tubes with flow coolant. The center white cell is deemed to be a guide tube for the process of calculation, even if it should be an instrumentation thimble in an actual reactor assembly. Considering the diagonal symmetry and reflection symmetry, one-eighth of the assembly is selected for simulation calculation. Tables 1 and 2 summarize the steady-state parameters for the PWR design.

2.3 Cladding models

Typical zirconium (Zr alloy) cladding is regarded as a reference case, and two types of SiC cladding assemblies are proposed for contrast: Simply, case one consists of SiC cladding with UO_2 fuel and case two is SiC cladding with UO_2/BeO fuel. Because of the low thermal conductivity of irradiated SiC material (one-third the thermal conductivity of irradiated zirconium alloy), case two explores the performance of a mixture of UO_2/BeO fuel. As a high-thermal conductivity material, BeO is used to keep SiC cladding fuel at a similar thermal conductivity as Zr alloy cladding fuel. Tables 3, 4, and 5 show the data in detail. The enrichment setting in Table 3 is used to maintain a uniform

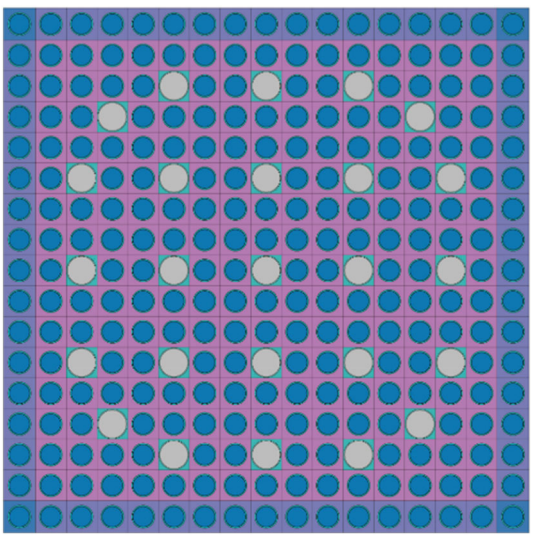

Fig. 1 (Color online) Structural arrangement of assemblies

Table 1 Fuel assembly parameters for SiC and Zr alloy cladding cases

Assembly parameter	SiC clad fuel	Zr alloy clad fuel
Fuel assembly rod array	17 × 17	17 × 17
Number of guide thimbles	24	24
Number of instrumentation thimbles	1	1
Pin-to-pin pitch (mm)	12.6	12.6
Number of fuel rods per assembly	264	264
Specific power (Kw/Kg)	39.98	39.98

Table 2 Reference design value for PWR

Gap conductance (W/m^2 K)	7500
Gap thickness (cm)	0.0103
Cladding thickness (cm)	0.057
Coolant velocity (m/s)	5.5

^{235}U load. Equations for enrichment calculation are shown as follows.

$$c_5 = \left(1 + 0.9874 \times \left(\frac{1}{\varepsilon} - 1\right)\right)^{-1} \quad (1)$$

$$M_{UO_2} = M_{U_{235}} \times c_5 + M_{U_{238}} \times (1 - c_5) + 2 \times M_O \quad (2)$$

$$\rho_m = v\%_{BeO} \times \rho_{BeO} + v\%_{UO_2} \times \rho_{UO_2} \quad (3)$$

$$wt_T\%_{UO_2} = \frac{v\%_{UO_2} \times \rho_{UO_2}}{\rho_m} \quad (4)$$

$$wt_T\%_U = wt_T\%_{UO_2} \times \frac{M_U}{M_{UO_2}} \quad (5)$$

$$wt_T\%_{^{235}U} = wt_T\%_U \times \varepsilon, \quad (6)$$

where c_5 is the number of ^{235}U nuclides divided by the sum of ^{235}U and ^{238}U nuclides;ε denotes enrichment of a fuel pellet; $wt_T\%$ is set as the volume ratio; and ρ_{UO_2} is 10.42 g/cm^3.

The setting of 0.089 cm for the thickness of UO_2/BeO cladding results from manufacturing technique used for SiC material in practical industrial production.

Six groups of temperature perturbations are adopted for moderator and fuel temperature coefficient calculation. Table 6 lists these temperature perturbations.

Table 4 Constituents of Zr alloy cladding and SiC cladding

Material	Fe	Cr	Zr alloy	Sn	Si	C
wt%						
Zircaloy	0.15	0.1	98.26	1.49		
SiC					70.08	29.92
at.%						
Zircaloy	0.24	0.17	98.43	1.15		
SiC					50	50

Table 5 UO_2/BeO analysis parameters

BeO at.%	9.51%
Density of BeO (g/cm^3)	2.85
Thermal conductivity for 100% UO_2	$257.99 \times T^{-0.627}$
Thermal conductivity for 90%UO_2 + 10%BeO	$497.6 \times T^{-0.679}$
Thermal conductivity for 91%UO_2 + 9%BeO	$443.32 \times T^{-0.67}$

3 Results and analysis

Neutronic parameters were analyzed for SiC cladding with the purpose of evaluating the assembly characteristics. What follows in this section includes the thermal neutron spectrum, characteristic factors (coefficient), influence of burnable poison rod power, and flux and power distributions.

3.1 Neutron spectrum and ^{239}Pu analysis

Figures 2 and 3 represent the neutron spectrum curves corresponding to the three cases. The computational

Table 3 Parameters for fuel cladding used in the analysis

	Zr alloy cladding	SiC cladding	SiC cladding with BeO
Cladding thickness (cm)	0.057	0.057	0.089
Enrichment (%)	3.393	3.393	3.749
Gap thickness (cm)	0.0103	0.0103	0.0103
Cladding density (g/cm^3)	6.55	2.58	2.58
Microscopic thermal neutron absorption cross section (barns)	0.20	0.086	0.086

Table 6 Perturbations for calculation of temperature coefficient of reactivity

Coolant temperature perturbation (K)		Fuel temperature perturbation (K)	
Case 1	Reference and case 2	Case 1	Reference and case 2
560	560	1235	1187
570	570	1285	1237
580	580	1335	1287
590	590	1385	1337
600	600	1435	1387
610	610	1485	1437

domain for the neutron flux was the perpendicular plane in the axial direction of the fuel rod.

Figure 2 shows the neutron spectrum in the range of 0–4 eV at the beginning of cycle (BOC). Zooming in on part of Fig. 2 (in the range of 0.1–0.62 eV), it clearly shows that Zr alloy case has a harder thermal neutron spectrum than the SiC case and SiC/BeO case. Similar to Figs. 2 and 3 presents the neutron spectrum at the end of cycle (EOC). Compared with Fig. 2, there is little flux disparity (in the range of 0.1 eV) observed in Fig. 3. In the meantime, the thermal neutron flux decreases at 0.1 eV. This is due to the depletion of the ^{235}U and accumulation of absorbent fission products. This effect becomes more prominent in the SiC case and SiC/BeO case because of their high thermal neutron peak at BOC. Lower neutron capture cross sections for the SiC material contribute to better thermal neutron spectrum performance, and a softer thermal neutron spectrum provides an economic advantage for a thermal neutron reactor.

In addition to the neutron spectrum study, the amount of ^{239}Pu is displayed in Fig. 4. The hardening thermal neutron spectrum in the Zr alloy case results in higher accumulation of ^{239}Pu. ^{239}Pu has a significant influence on the reactivity.

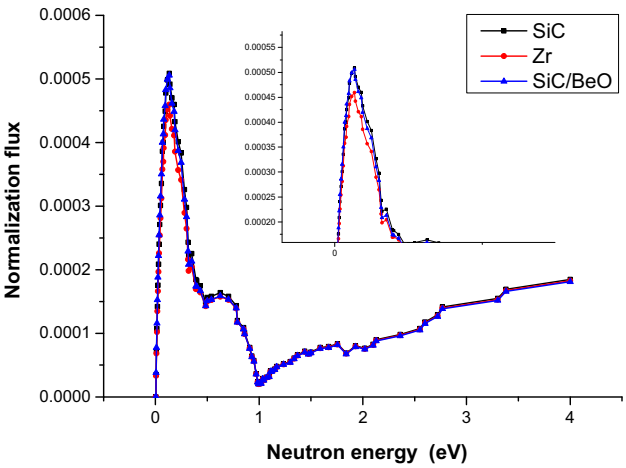

Fig. 3 (Color online) Thermal neutron spectrum at the end of cycle

Therefore, it may contribute to a slight reactive increase in EOC.

3.2 Characteristic factor results

Enrichment analysis was carried out by comparing infinite multiplication factors. Two kinds of fuel assemblies

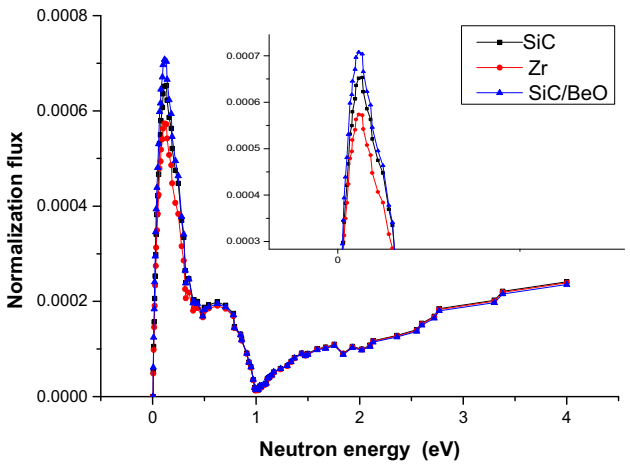

Fig. 2 (Color online) Thermal neutron spectrum at the beginning of cycle

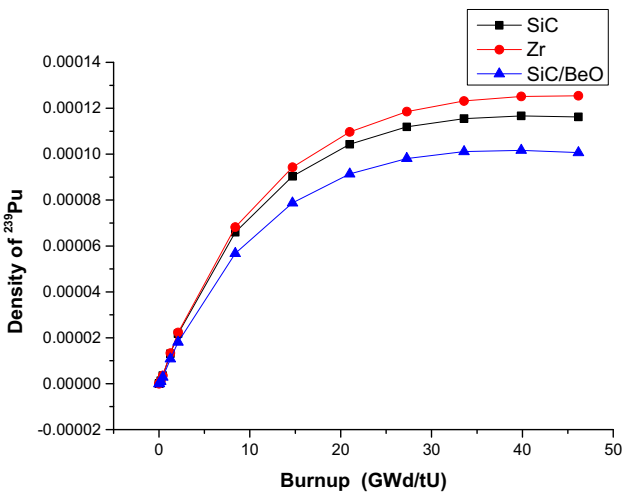

Fig. 4 (Color online) ^{239}Pu content

were involved for implementing enrichment analysis. Enrichment in the SiC case and initial Zr alloy case was 3.393%. Increasing enrichment stepwise by 0.5% in six other Zr alloy case groups, there are seven groups of Zr alloy cases in total. Other parameters remain unchanged, in accordance with Table 3.

Figure 5 shows that all curves have a similar tendency as a function of burnup. Detailed drawings are inserted in Fig. 5. In the beginning, the SiC case is quite close to that of Zr alloy (3.643%). The fluctuate part of the curve in this stage results from xenon poisoning. Because of the rapid drop in the SiC curve, its Kinf is close to that of Zr alloy (3.443%) in the end. Depending on the burnup level, the reduction value of enrichment is approximately 0.05–0.25%. In the case where no power control is applied, a softer thermal neutron spectrum leads to more speedy consumption of ^{235}U in the SiC assembly.

Furthermore, by inserting an amount of burnable poison rods in the assemblies, the impact of burnable poison control was analyzed, as discussed in the subsequent paragraph.

Figure 6 shows the plot of Kinf when various numbers of burnable poison rods are inserted in assemblies. The results obviously demonstrate that as more burnable poison rods were inserted in the SiC cladding assembly, the Kinf value that appears at the early stage decreased. A quite similar trend is observed regarding the SiC case and Zr alloy case. This result demonstrates that conventional burnable poison rods maintain a favorable regulating effect on SiC cladding assemblies.

Figure 7 shows the power peak factor (Ppf) for various assemblies. The SiC/BeO case has the highest power peak factor. Zr alloy cladding has a Ppf that is slightly higher than that of SiC cladding. All of the curves increase in the early stage. Because of the negative feedback associated with the fuel rod power, the value of Ppf decreases slowly

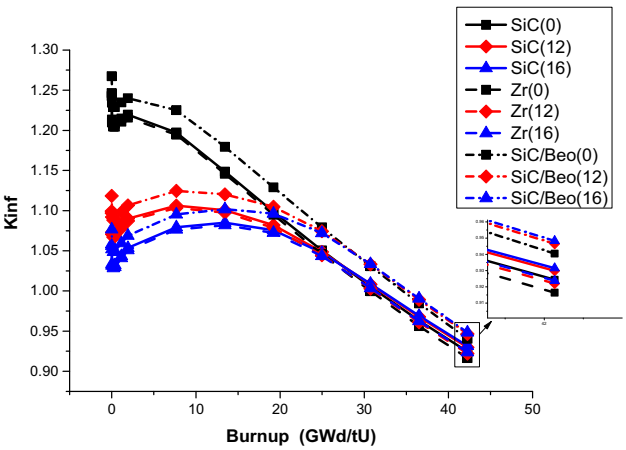

Fig. 6 (Color online) Kinf in various assemblies with burnable poison rod

at later stages. The curve for the SiC case is consistent with that for the Zr alloy case. This result means that the SiC case would cause few operational changes from the perspective of controlling power distribution. Additionally, Zr alloy case has a higher Ppf than SiC cladding as the burnup progresses. The performance of the SiC case reveals its ability to flatten the power distribution within the assemblies. The relatively poor performance in the SiC/BeO case may be caused by its thicker cladding and the addition of BeO.

The relative power distribution at BOC in the SiC case assembly is presented in Fig. 8. All values have been normalized. Figure 8 clearly describes the relative power distribution in the assembly. It is easy to see that regions close to the water rod possess low power. Additionally, Fig. 9 describes the relative power transformation between BOC and EOC. In contrast to the BOC power, the green parts in Fig. 9 stand for areas where power decreases, and the orange parts correspond to areas where the power

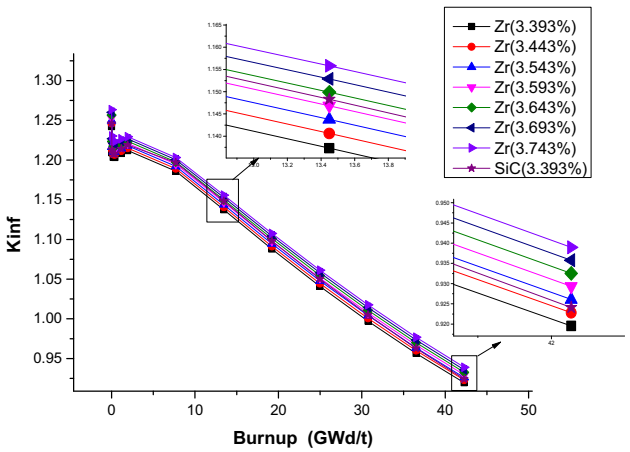

Fig. 5 (Color online) Trend of Kinf in assemblies with various enrichments

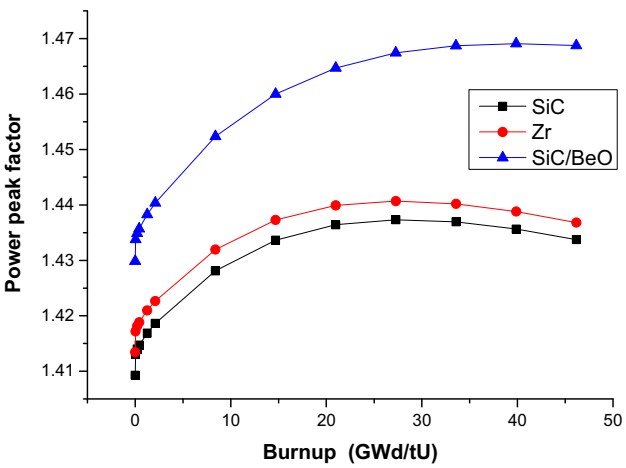

Fig. 7 (Color online) Ppf for various assemblies

increases. In the process of burnup, the power in the exterior zone would increase while the power in the interior area decreases. This phenomenon is due to the faster depletion of ^{235}U inside the assembly than in the exterior assembly.

3.3 Radial profile analysis

Differences in the neutron absorption ability of cladding material would lead to radial differentiations in fuel pellets [26, 27]. The radial flux distribution is explored in four areas by segmenting the inner UO_2 pellet into four equal concentric annuli. The innermost concentric annulus is called Part 1, and the others are called Parts 2, 3, and 4 in turn. Regions in Fig. 8 that are surrounded by black bold squares with marked numbers are chosen for analysis (specific to the SiC assembly).

Figure 10 describes the normalization flux in the four regions in the SiC cladding assembly fuel pellet. The four regions have a similar tendency overall. Nearby water rod regions have highest flux in Part 1. Others have the highest flux in Part 4. Part 2 in the marginal area (Region 1) has less flux value compared with the interior area (Region 4). This result shows that the layout of the water rod and boundary interference can affect the radial flux distribution in fuel pellets.

Figures 11 and 12 show the relative fission power distribution in fuel pellets. From Figs. 11 and 12, similar trends among these three cases can be observed. Because of the spatial self-shielding that may prevent thermal neutrons from penetrating to the inner fuel pellet, the outer part of the fuel pellet possesses higher fission power. Also, as burnup proceeds, spatial self-shielding leads to an increase in the plutonium produced in the outer fuel pellet. Accumulation of extra fission material makes the slope of the curves in Fig. 12 steeper than that in Fig. 11. The Zr alloy

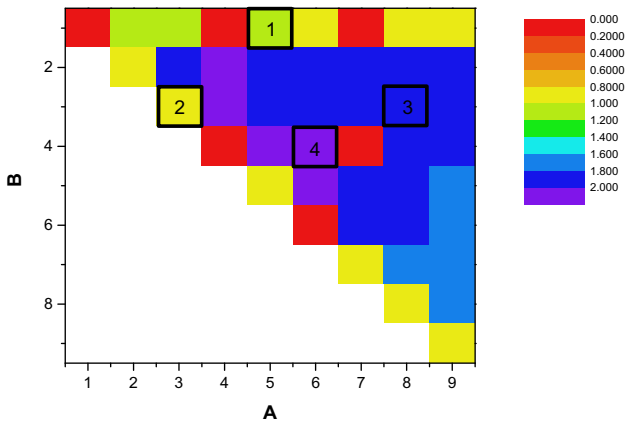

Fig. 8 (Color online) Distribution of relative power in SiC cladding assembly at the beginning of cycle

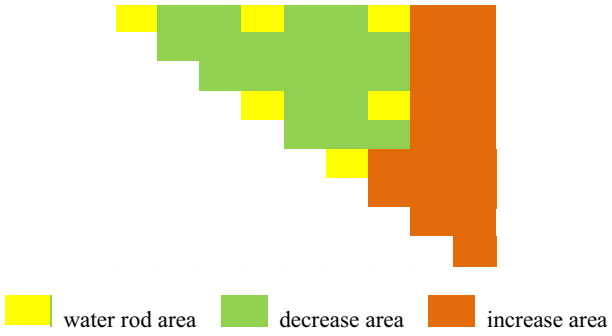

Fig. 9 (Color online) Power variation in SiC cladding assembly at the end of cycle

case has the smallest fission power at BOC and the largest at EOC. This is due to the higher thermal neutron capture cross section in Zr alloy material, which is more likely to block thermal neutrons and slow down the outside moderator at BOC. Nevertheless, the harder neutron spectrum in the Zr alloy case results in the production of more plutonium in the outer fuel pellet. The additional fission material would increase the relative fission power at later stages. Unavoidably, compared with the Monte Carlo method, the accuracy of DRAGON for radial power calculation may be lower, although a revised resonance self-shielding calculation modular and fine neutron energy groups in DRAGON may partially compensate for this. There has been some excellent research in this field using Monte Carlo methods [28, 29].

3.4 Moderator temperature coefficient analysis

Respectively, Figs. 13 and 14 describe the moderator and fuel temperature coefficients as a function of burnup. The moderator and fuel temperature coefficients appear in the following equation:

$$\partial = \frac{\Delta\rho}{\Delta T}, \tag{7}$$

where ∂ is the temperature coefficient, $\Delta\rho$ is the reactivity difference, and ΔT stands for temperature difference. As shown in Table 6, ΔT is equal to 10 K for the moderator temperature coefficient (MTC) calculation, while it is 50 K for the fuel temperature coefficient (FTC) calculation.

Figure 13 reveals that three kinds of assemblies show negative MTC during the overall burnup period. There is no obvious difference in the early stage. In the intermediate stage, the SiC/BeO case has a more strongly negative coefficient than the other cases. Conversely, the SiC case has the weakest negative coefficient. The feedback coefficient in the SiC/BeO case becomes weaker at later stages. The Zr alloy case has a strongly negative coefficient. Because of the depletion of ^{235}U, which relatively

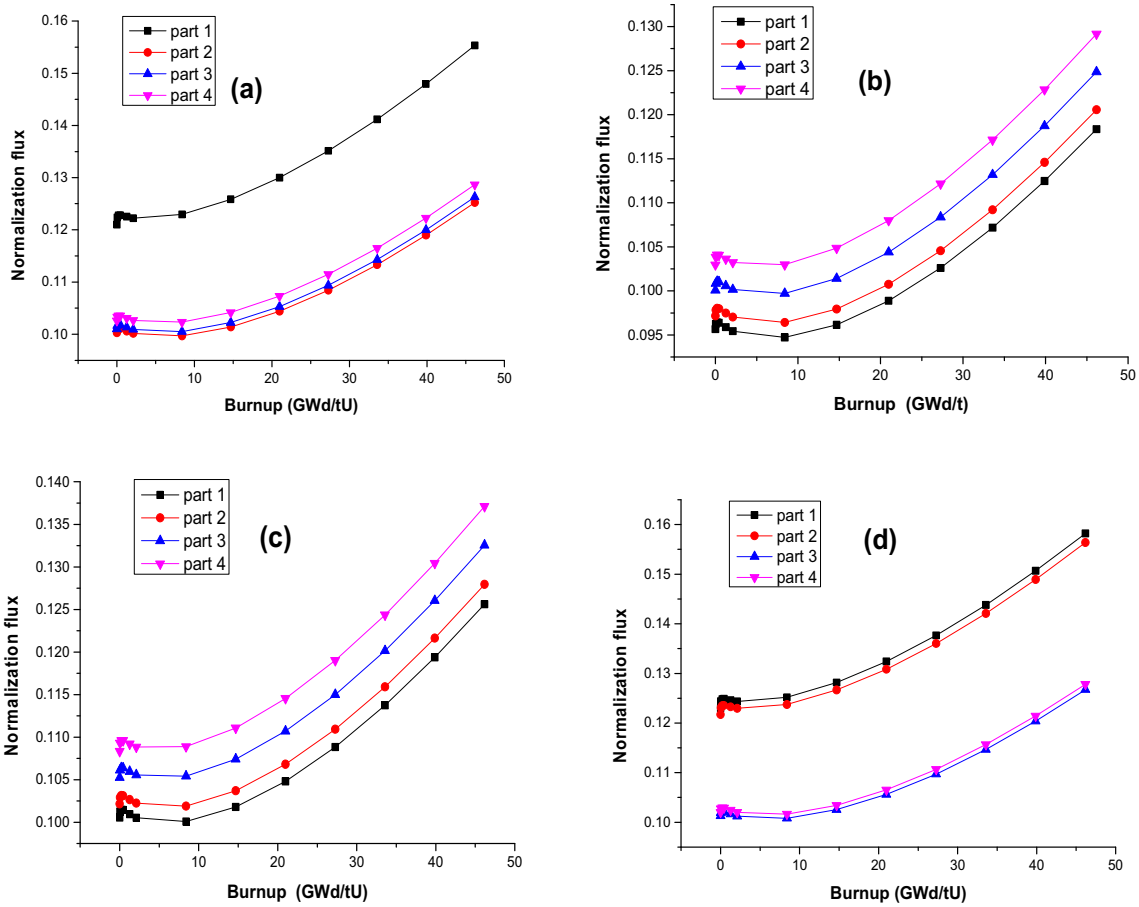

Fig. 10 (Color online) Normalization flux in four parts. **a** Flux in region one, **b** flux in region two, **c** flux in region three, **d** flux in region four

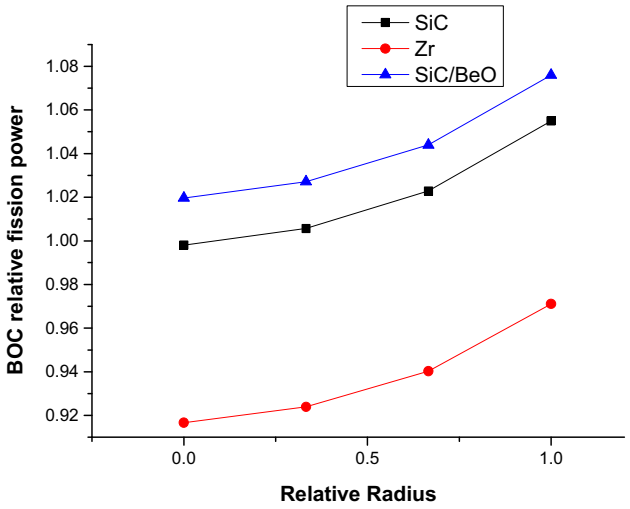

Fig. 11 (Color online) Relative radial power distribution at the beginning of cycle

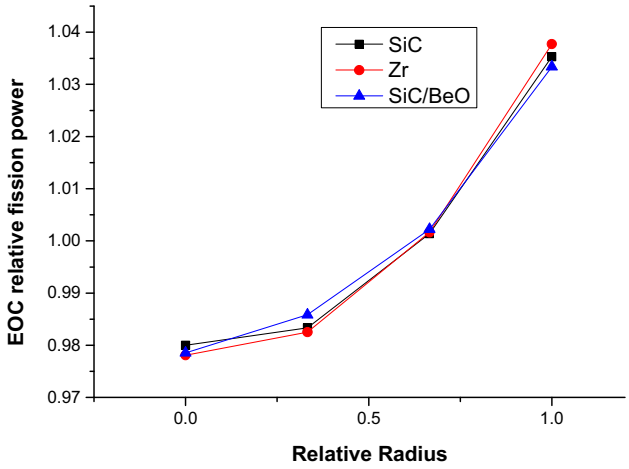

Fig. 12 (Color online) Relative radial power distribution at the end of cycle

enhances the ^{238}U resonance absorption, the MTC becomes more sensitive to changes in the moderator temperature and density. Nevertheless, accumulation of fission products at the later period leads to a less negative MTC value.

Figure 14 shows the trend for the FTC. For the SiC case, there is a strongly negative feedback coefficient throughout the burnup progress. The Zr alloy case has the weakest value. The lower absolute value of FTC is a result of the

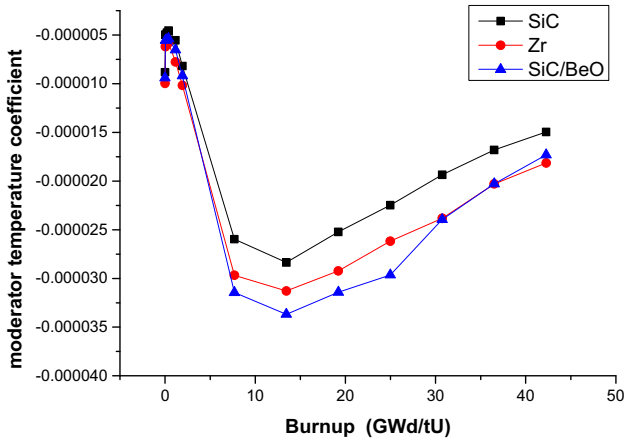

Fig. 13 (Color online) Moderator temperature coefficient

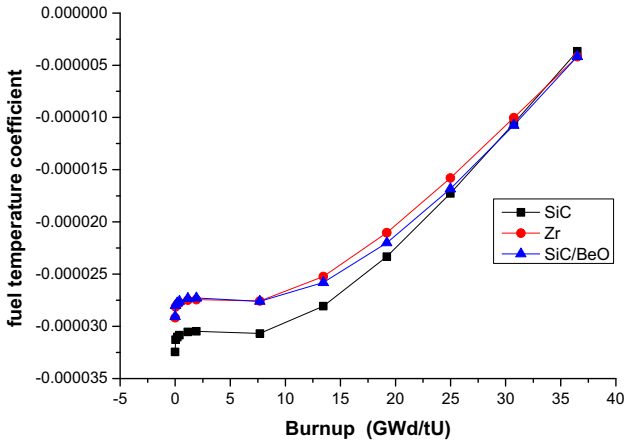

Fig. 14 (Color online) Fuel temperature coefficient

influence of ^{239}Pu and ^{241}Pu and the contribution of the reduced resonance absorption.

The fuel and moderator temperature coefficients are the two most important elements of the reactor feedback coefficient. Figure 15 combines these two temperature coefficients into one total feedback coefficient. For a short time in the early stage, the SiC case has the most strongly negative coefficient. The SiC/BeO case has strong feedback in middle of cycle (MOC). As burnup increases, the SiC and SiC/BeO cases have weaker negative feedback coefficients than the Zr alloy case. To briefly summarize the temperature feedback coefficient results, in a reasonable range, the SiC case has the weakest negative MTC and most strongly negative FTC. SiC and SiC/BeO cases have a more strongly negative feedback coefficient in the early burnup stage. At later stages of burnup, the most strongly negative coefficient is observed in the Zr alloy case. The positive reactivity coefficient brought about by SiC cladding should be given more attention.

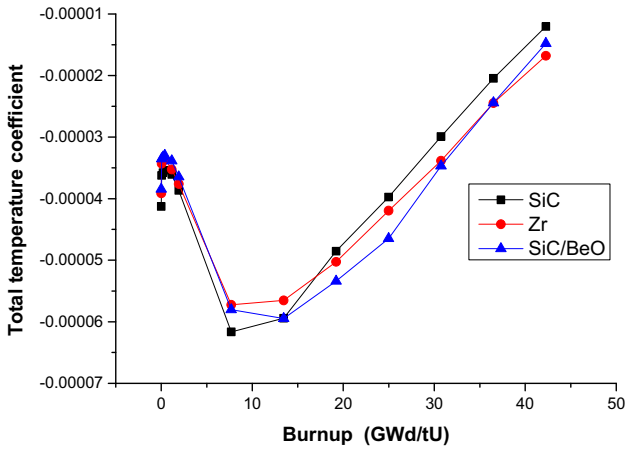

Fig. 15 (Color online) Total temperature coefficient

4 Conclusion

Neutron analysis with respect to SiC cladding fuel assemblies was implemented. Characteristic parameters, with the exception of power distribution at the beginning of cycle and inner UO_2 pellet flux and fission power distribution, were compared with a Zr alloy cladding assembly. In addition, fuel enrichment and normalization power transformation in the assembly were discussed. SiC cladding fuel and SiC cladding with UO_2/BeO fuel have quite similar neutronic performances.

Neutron spectral analysis reveals that the SiC cladding fuel assembly has a softer thermal neutron spectrum than the Zr alloy cladding fuel assembly, which results in less ^{239}Pu accumulation in the SiC cladding assembly. The analytic results for the neutronic parameters demonstrate that the SiC cladding assemblies have the advantage of reducing the necessary fuel enrichment and a favorable, flattened distribution. The low neutron capture ability of SiC cladding assemblies is conducive to extend discharge burnup. A softer thermal neutron spectrum allows a larger fuel pin lattice space without an apparent reactivity penalty. The flux trend in four parts of the SiC cladding assembly reveals that the water rod and boundary interference would have an effect on the radial flux distribution. The influence of different kinds of cladding materials on the fission power distribution in fuel pellets is limited. Within the scope of security, temperature coefficient analysis demonstrated that SiC cladding assemblies maintain a negative coefficient, even if the reactivity coefficient is slightly positive. Generally, the similar neutronic performances between SiC cladding assemblies and Zr alloy cladding assemblies are a benefit for cladding substitution

with few changes to reactor operation. Moreover, the SiC cladding assemblies display a high neutron economy and reliability.

References

1. L.J. Ott, K.R. Robb, D. Wang, Preliminary assessment of accident-tolerant fuels on LWR performance during normal operation and under DB and BDB accident conditions. J. Nucl. Mater. **448**, 520–533 (2014). https://doi.org/10.1016/j.jnucmat.2013.09.052
2. S.J. Zinkle, K.A. Terrani, J.C. Gehin et al., Accident tolerant fuels for LWRs: a perspective. J. Nucl. Mater. **448**, 374–379 (2014). https://doi.org/10.1016/j.jnucmat.2013.12.005
3. N.R. Brown, H. Ludewig, A. Aronson et al., Neutronic evaluation of a PWR with fully ceramic microencapsulated fuel. Part II: nodal core calculations and preliminary study of thermal hydraulic feedback. Ann. Nucl. Energy **62**, 548–557 (2013). https://doi.org/10.1016/j.anucene.2013.05.027
4. N.R. Brown, H. Ludewig, A. Aronson et al., Neutronic evaluation of a PWR with fully ceramic microencapsulated fuel. Part I: Lattice benchmarking, cycle length, and reactivity coefficients. Ann. Nucl. Energy **62**, 538–547 (2013). https://doi.org/10.1016/j.anucene.2013.05.025
5. H. Ahmed, K.S. Chaudri, S.M. Mirza, Comparative analyses of coated and composite UN fuel—Monte Carlo based full core LWR study. Prog. Nucl. Energy **93**, 260–266 (2016). https://doi.org/10.1016/j.pnucene.2016.08.014
6. X. Wu, T. Kozlowski, J.D. Hales, Neutronics and fuel performance evaluation of accident tolerant FeCrAl cladding under normal operation conditions. Ann. Nucl. Energy **85**, 763–775 (2014). https://doi.org/10.1016/j.anucene.2015.06.032
7. N.M. George, K. Terrani, J. Powers et al., Neutronic analysis of candidate accident-tolerant cladding concepts in pressurized water reactors. Ann. Nucl. Energy **75**, 703–712 (2015). https://doi.org/10.1016/j.anucene.2014.09.005
8. I. Younker, M. Fratoni, Neutronic evaluation of coating and cladding materials for accident tolerant fuels. Prog. Nucl. Energy **88**, 10–18 (2016). https://doi.org/10.1016/j.pnucene.2015.11.006
9. S.M. Bragg-Sitton, *Light Water Reactor Sustainability Program. Advanced LWR Nuclear Fuel Cladding System Development Technical Program Plan*, INL/MIS-12e. 25696 (2012)
10. Y. Liu, I. Bhamji, P.J. Withers et al., Evaluation of the interfacial shear strength and residual stress of TiAlN coating on ZIRLO^{TM} fuel cladding using a modified shear-lag model approach. J. Nucl. Mater. **65**, 718–727 (2015). https://doi.org/10.1016/j.jnucmat.2015.06.003
11. N.R. Brown, A.J. Wysocki, K.A. Terrani et al., The potential impact of enhanced accident tolerant cladding materials on reactivity initiated accidents in light water reactors. Ann. Nucl. Energy **99**, 353–365 (2017). https://doi.org/10.1016/j.anucene.2016.09.033
12. X. Wu, W. Li, Y. Wang et al., Preliminary safety analysis of the PWR with accident-tolerant fuels during severe accident conditions. Ann. Nucl. Energy **80**, 1–13 (2015). https://doi.org/10.1016/j.anucene.2015.02.040
13. Y. Katoh, K. Ozawa, C. Shih et al., Continuous SiC fiber, CVI SiC matrix composites for nuclear applications: properties and irradiation effects. J. Nucl. Mater. **448**, 448–476 (2014). https://doi.org/10.1016/j.jnucmat.2013.06.040
14. Y. Deng, Y. Wu, B. Qiu et al., Development of a new Pellet-Clad Mechanical Interaction (PCMI) model and its application in ATFs. Ann. Nucl. Energy **104**, 146–156 (2017). https://doi.org/10.1016/j.anucene.2017.02.022
15. D.A. Bloore, *Reactor Physics Assessment of Thick Silicon Carbide Clad PWR Fuels* (2013). http://hdl.handle.net/1721.1/82454
16. D.M. Carpenter, *An Assessment of Silicon Carbide as a Cladding Material for Light Water Reactors* (2010). http://hdl.handle.net/1721.1/76975
17. H. Matsumiya, K. Yoshioka, T. Kikuchi et al., Reactivity measurements of SiC for accident-tolerant fuel. Prog. Nucl. Energy **82**, 16–21 (2015). https://doi.org/10.1016/j.pnucene.2014.07.030
18. M. Kromar, B. Kurinčič, DRAGON and CORD-2 nuclear calculation of the NPP Krško fuel assembly. Nucl. Eng. Des. **246**, 58–62 (2012). https://doi.org/10.1016/j.nucengdes.2011.06.043
19. S. Liu, J. Cai, Neutronic and thermohydraulic characteristics of a new breeding thorium–uranium mixed SCWR fuel assembly. Ann. Nucl. Energy **62**, 429–436 (2013). https://doi.org/10.1016/j.anucene.2013.07.004
20. S. Liu, J. Cai, Studies of fuel loading pattern optimization for a typical pressurized water reactor (PWR) using improved pivot particle swarm method. Ann. Nucl. Energy **50**, 117–125 (2012). https://doi.org/10.1016/j.anucene.2012.08.007
21. S. Liu, J. Cai, Design & optimization of two breeding thorium–uranium mixed SCWR fuel assemblies. Prog. Nucl. Energy **70**, 6–19 (2014). https://doi.org/10.1016/j.pnucene.2013.07.011
22. A. Naceur, G. Marleau, Neutronic analysis for accident tolerant cladding candidates in CANDU-6 reactors. Ann. Nucl. Energy **113**, 147–161 (2018). https://doi.org/10.1016/j.anucene.2017.11.016
23. Y. Katoh, T. Nozawa, L.L. Snead, K. Ozawa, H. Tanigawa, Stability of SiC and its composites at high neutron fluence. J. Nucl. Mater. **417**, 400–405 (2011). https://doi.org/10.1016/j.jnucmat.2010.12.088
24. K.A. Terrani, J.R. Keiser, M.P. Brady, et al., *High Temperature Oxidation of Silicon Carbide and Advanced Iron-Based Alloys in Steam-Hydrogen Environments* (2012). https://www.osti.gov/biblio/1055072
25. T. Cheng, J.R. Keiser, M.P. Brady et al., Oxidation of fuel cladding candidate materials in steam environments at high temperature and pressure. J. Nucl. Mater. **427**, 396–400 (2012). https://doi.org/10.1016/j.jnucmat.2012.05.007
26. M.H.A. Piro, J. Banfield, K.T. Clarno et al., Coupled thermo-chemical, isotopic evolution and heat transfer simulations in highly irradiated UO_2 nuclear fuel. J. Nucl. Mater. **441**, 240–251 (2013). https://doi.org/10.1016/j.jnucmat.2013.05.060
27. D. Baron, M. Kinoshita, P. Thevenin et al., Discussion about HBS transformation in high burn-up fuels. Nucl. Eng. Technol. **41**, 199–214 (2009). https://doi.org/10.5516/net.2009.41.2.199
28. S. Chen, C. Yuan, Neutronic analysis on potential accident tolerant fuel-cladding combination U3Si2-FeCrAl, in *Science and Technology and Nuclear Installations*, 2017, (2017-01-18) (2017), pp. 1–12
29. Recently, U.O. The, A simple formula for local burnup and isotope distributions based on approximately constant relative reaction rate, in *Science and Technology and Nuclear Installations*, 2016, (2016-2-17) (2016), pp. 1–8